Regular paper

Protective effects of fatty acid amide hydrolase inhibition in UVB-activated microglia

Veronica Carnicelli [a,1], Noemi De Dominicis [a,b,1], Lucia Scipioni [a,c], Marina Fava [d], Federico Fanti [e], Benedetta Cinque [f], Alessandro Leuti [c,d], Clotilde Beatrice Angelucci [g], Anna Rita Lizzi [a], Roberto Giacominelli-Stuffler [g], Vincenzo Flati [a], Manuel Sergi [h], Dario Compagnone [e], Anna Maria Sardanelli [i,2], Annamaria Tisi [a], Sergio Oddi [c,g,*,2], Mauro Maccarrone [a,c,**,2]

[a] Department of Biotechnological and Applied Clinical Sciences, University of L'Aquila, 67100 L'Aquila, Italy
[b] Department of Physics, University of Trento, 38123 Trento, Italy
[c] European Center for Brain Research/IRCCS Santa Lucia Foundation, 00143 Rome, Italy
[d] Department of Medicine, Campus Bio-Medico University of Rome, 00128 Rome, Italy
[e] Department of Bioscience and Technology for Agriculture, Food and Environment, Campus Universitario di Coste Sant'Agostino, University of Teramo, Italy
[f] Department of Life, Health & Environmental Sciences, University of L'Aquila, 67100 L'Aquila, Italy
[g] Department of Veterinary Medicine, University of Teramo, 64100 Teramo, Italy
[h] Department of Chemistry, Sapienza University of Rome, Rome, Italy
[i] Department of Translational Biomedicine and Neuroscience 'DiBraiN', University of Bari "Aldo Moro", 70121 Bari, Italy

ARTICLE INFO

ABSTRACT

Neuroinflammation is a hallmark of several neurodegenerative disorders that has been extensively studied in recent years. Microglia, the primary immune cells of the central nervous system (CNS), are key players in this physiological process, demonstrating a remarkable adaptability in responding to various stimuli in the eye and the brain. Within the complex network of neuroinflammatory signals, the fatty acid *N*-ethanolamines, in particular *N*-arachidonylethanolamine (anandamide, AEA), emerged as crucial regulators of microglial activity under both physiological and pathological states. In this study, we interrogated for the first time the impact of the signaling of these bioactive lipids on microglial cell responses to a sub-lethal acute UVB radiation, a physical stressor responsible of microglia reactivity in either the retina or the brain. To this end, we developed an in vitro model using mouse microglial BV-2 cells. Upon 24 h of UVB exposure, BV-2 cells showed elevated oxidative stress markers and, cyclooxygenase (COX-2) expression, enhanced phagocytic and chemotactic activities, along with an altered immune profiling. Notably, UVB exposure led to a selective increase in expression and activity of fatty acid amide hydrolase (FAAH), the main enzyme responsible for degradation of fatty acid ethanolamides. Pharmacological FAAH inhibition via URB597 counteracted the effects of UVB exposure, decreasing tumor necrosis factor α (TNF-α) and nitric oxide (NO) release and reverting reactive oxidative species (ROS), interleukin-1β (IL-1β), and interleukin-10 (IL-10) levels to the control levels. Our findings support the potential of enhanced fatty acid amide signaling in mitigating UVB-induced cellular damage, paving the way to further exploration of these lipids in light-induced immune responses.

* Correspondence to: S. Oddi, European Center for Brain Research/IRCCS Santa Lucia Foundation, 00143 Rome, Italy.
** Correspondence to: M. Maccarrone, Department of Biotechnological and Applied Clinical Sciences, University of L'Aquila, 67100 L'Aquila, Italy.
  E-mail addresses: soddi@unite.it (S. Oddi), mauro.maccarrone@univaq.it (M. Maccarrone).
[1] These authors contributed equally.
[2] Co-senior authors

1. Introduction

The recent scientific debate has focused on neuroinflammation, a key feature of many neurodegenerative disorders. Neuroinflammation occurs when resident immune cells, primarily microglia, are activated in response to different triggers such as injury, infection, or exposure to toxic substances [1]. Physiologically, microglial cells play vital roles in helping the brain to restore the homeostasis of the nervous tissue and protecting various cell types, including neurons [2–4] and retinal photoreceptors [5–7] from detrimental and inflammatory insults.

One interesting characteristic of microglia is their ability to adapt. When exposed to different stimuli, microglial cells can undergo dynamic changes in their phenotypic and functional activity, demonstrating their importance in the immune response within the brain. Yet, exposure to certain (bio)chemicals, such as bacterial lipopolysaccharides (LPS), or physical factors such as UV light [8], can cause microglia to switch to a specific phenotype called M1, which leads to the onset of oxidative stress and the production of pro-inflammatory cytokines. These events are initially induced as a self-protective mechanism; however, dysfunction and prolonged microglia activation finally contribute and are associated with neurodegenerative disorders of the brain and the eye [9–11].

From a molecular perspective, several cellular signal transduction systems coordinate and control each of these processes, enabling microglial cells to respond effectively to a range of endogenous and/or exogenous stressors. Within this defense system, the endocannabinoids (eCBs) AEA [12] and 2-arachidonoylglycerol (2-AG) [13] have a crucial role in regulating microglial activity under normal and pathological conditions [14]. AEA and 2-AG belong to the so called "endocannabinoid system" (ECS), that consists of several eCBs, their metabolic enzymes and receptor targets [15]. Acylethanolamides other than AEA, like palmitoylethanolamide (PEA) and oleoylethanolamide (OEA), are considered eCB-like compounds, as they do not directly activate cannabinoid receptors but interact with other targets able to influence the eCB signaling [16]. Briefly, AEA is produced by *N*-arachidonoyl phosphatidylethanolamines-specific phospholipase D (NAPE-PLD) [17,18] and is degraded by FAAH [19]. In relation to the latter, fatty acid amide hydrolase-2 (FAAH-2) [20,21] and N-acylethanolamine-hydrolyzing acid amidase (NAAA) [22,23], are additional enzymes that may also bind to acylethanolamides with lower affinity and hydrolyze it [24].

On the other hand, 2-AG is synthetized by diacylglycerol lipases α and β (DAGLα/β) [25] and is degraded by monoacylglycerol lipase (MAGL) [26] which was found the primary 2-AG hydrolase in mouse brain. In addition, a minor activity was attributable to other two enzymes, α/β-hydrolase-6 (ABDH-6) and α/β-hydrolase-12 (ABDH-12) [27].

Furthermore, distinct lipoxygenase (LOX) isozymes, cytochrome P450, and COX-2 can oxidize AEA and 2-AG [27,28].

The G protein-coupled cannabinoid 1 and 2 (CB$_1$ and CB$_2$) receptors are the main targets of eCBs, that can also bind to additional non-cannabinoid receptors like the orphan G-coupled receptor GPR55, the transient receptor potential vanilloid type-1 (TRPV1) ion channel, and the peroxisome proliferator-activated nuclear receptors (PPARs) [15]. This biochemical system is expressed by microglia, where it regulates the immune activity by driving release of pro- and anti-inflammatory mediators, as well as cell proliferation, migration, and phagocytosis [14,29]. In particular, AEA, alone or in combination with PEA and OEA, triggers signaling activity that has been linked to the control of cellular responses to a variety of stresses and insults, such as inflammation [30], heat stress [31], excitotoxic stress [32], and exposure to ultraviolet (UV) radiation [33,34]. Through its key regulatory impact on microglia physiology [14,35], this lipid signaling appears to be particularly important in the neuroinflammatory response.

In the present study, for the first time we interrogated the influence of FAAH activity on cellular responses to UVB radiation, a physical stressor to which microglial cells are exposed in the retina. To this end, we developed and characterized an in vitro model that induces a sublethal acute UVB damage in BV-2 cells, a widely used immortalized mouse microglial cell line. By pharmacologically inhibiting FAAH we primarily manipulated endogenous fatty acid amide signaling to explore its potential in attenuating UVB-induced cellular changes.

2. Materials and methods

2.1. Chemicals

DMEM with and without phenol red was purchased from Euroclone (Pero, Milan, IT), as well as other cell culture reagents. Non-treated plasticware was purchased from Starlab (Starlab International GmbH, Hamburg, DE). The 2′,7′-dichlorodihydrofluorescein diacetate probe and the inhibitor URB597 substance were obtained from Molecular Probes, (Eugene, OR, USA). Nitric oxide was determined using the kit from Enzo Life Sciences (Enzo Life Sciences, Inc., Farmingdale, NY, USA). ELISA kits were purchased from: Biolegend Inc. (BioLegend Way, San Diego, CA, USA) for TNF-α, PeproTech (Rocky Hill, NJ, USA) for IL-6, whereas the kits for IL-1β and IL-10 were from Invitrogen (Thermo Fisher Scientific, Inc., Waltham, MA, USA). The Aβ (1–42) FITC peptide was from AnaSpec (AnaSpec Inc. & Eurogentec US, Fremont, CA, USA). The Thincert cell culture system was purchased from Greiner Bio-One Italia S.r.l. (Milan, IT). The ReliaPrep RNA Miniprep System kit was from Promega (Milan, IT), whereas the Wonder RT cDNA Synthesis kit was purchased from Euroclone (Pero, Milan, IT). TaqMan Gene Expression Assays were obtained from ThermoFisher Scientific (Waltham, MA, USA). Arachidonic 7-amino-4-methyl coumarin amide, anti-CB$_2$ and anti-CB$_1$ primary antibodies were purchased from Cayman Chemicals, whilst the anti-TRPV1 primary antibody was from OriGene (OriGene Technologies, Inc., Rockville, MD, USA). Anti-GPR55, -PPARα, -PPARγ, -PPARδ, -FAAH, -COX-2 and -MAGL primary antibodies were purchased from Abcam (Cambridge, UK). Anti-DAGLα, -NAPE-PLD and -DAGLβ primary antibodies, as well as HRP-conjugated secondary antibodies, were from Thermo Scientific Pierce (Rockford, IL, USA). Anti-Iba1 was from Antibodies (Stockhlom, Sweden). The polyvinylidene fluoride (PVDF) membrane and the non-fat milk were from Bio-Rad (Bio-Rad Laboratories S.r.l., Segrate Milano, IT). All the other reagents were purchased from Sigma-Aldrich (St. Louis, MO, USA). The UVB lamp was purchased from Ditta Ammirata (Milan, IT).

2.2. Cell culture and treatments

The BV-2 microglial cell line, kindly provided by Dr. Mangino, Sapienza University of Rome, was grown in DMEM supplemented with 10 % Fetal Bovine Serum, 2 mM L-glutamine, 1 % penicillin-streptomycin and kept at 37 °C in a humidified atmosphere of 5 % CO$_2$. Cells were seeded at 4×10^3 cells/cm^2 density for each experiment in DMEM without phenol red and 24 h after plating, cells were irradiated with different UVB light doses (45, 75, 120, 150, 180 and 225 mJ/cm^2). We used the lamp UV-B Narrowband TL 20 W/01 RS SLV/25 (312 nm) at height 30 cm. The power (W) was measured with an UV radiometer and the doses were obtained by multiplying the power for the different irradiation times. We chose the dose of 153 mJ/cm^2 (ID50) for all experiments; control cells were protected with foil paper to prevent light exposure. In the FAAH inhibition experiments, cells were treated with: (i) UVB, (ii) 5 μM URB597, and (iii) UVB with 5 μM URB597. Notably, the addition of the drug occurred immediately after irradiation. Consequently, there was no necessity to monitor the chemical stability of the drug. All the analyses were conducted after 24 h.

2.3. Cell viability assays

Cell viability was assessed with the MTT assay. The cells were plated onto 96-well plate, at a density of 2.5×10^3 cells/well and exposed to UVB irradiation as aforementioned. The cell viability was assessed at 24

h post-irradiation. MTT was added to the wells to a final concentration of 0.5 mg/mL at 37 °C. The reaction was stopped after 45 min by adding 2-propanol-0.04 N HCl to the wells in a 1:1 ratio and pipetting to dissolve the crystals. The resulting colorimetric reaction was read in absorbance by means of a microplate reader (Tecan Infinite® 200 PRO). The cell viability was calculated by subtracting the 630 nm OD background from the 570 nm [36]. OD total signal of the cell-free blank of each sample and was expressed as percentage of the control (100 %).

2.4. Cell cycle distribution and apoptotic cells detection by flow cytometry

Cells were seeded in 100 × 20 mm Petri Dishes at 4×10^3 cells/cm^2 density. Control and treated BV-2 cells were collected, washed twice with ice-cold PBS, and fixed in 70 % ethanol solution at 4 °C for 30 min. Fixed cells (10^6 cells/mL) were then washed twice with ice-cold PBS and stained with a solution containing 50 µg/mL PI, 0.1 % Nonidet-P40, and RNase A (6 µg/10^6 cell) for 1 h in the dark at 4 °C. Data from 10,000 events per sample were collected and analyzed using a FACS Calibur instrument (BD Biosciences) equipped with cell cycle analysis software (Modfit LT for Mac V3.0) to calculate the percentages of cells in the G1, G2/M, and S phases. The apoptotic cells were determined by their hypochromic subdiploid nuclei staining profiles and analyzed using the Cell Quest software program (BD Instruments Inc., San José, CA, USA).

2.5. Intracellular ROS production

Cells were seeded in 100 × 20 mm Petri Dishes at 4×10^3 cells/cm^2 density. The level of intracellular ROS was measured at 24 h post-UVB with the probe 2′,7′-dichlorodihydrofluorescein diacetate (DCFH-DA). Briefly, the untreated and the irradiated BV-2 cells were incubated with 10 µM DCFH-DA at 37 °C for 30 min in darkness. Then, the cells were washed twice in ice-cold PBS, and then the fluorescence intensity was measured by spectrofluorometer (Perkin-Elmer LS-50B) setting excitation and emission wavelengths at 502 and 523 nm, respectively [37]. Data are expressed in arbitrary units (a.u.).

2.6. Nitric oxide determination

Cells were seeded in 24-well-plates at 4×10^3 cells/cm^2 density and the supernatants were collected from untreated BV-2 cells, as well as from BV-2 cells exposed to UVB or to URB597 alone and to both UVB and URB597. NO was quantified by measuring the nitrite concentration using the nitric oxide (NO_2-NO_3) detection kit according to the manufacturer's protocols. Standard and samples (80 µL) were added into 96-well plates and mixed to the nitrate reductase enzyme. The absorbance was read at 570 nm with a microplate reader (Tecan Infinite® 200 PRO). The amount of nitrite was calculated from the standard curves and data are expressed in µM.

2.7. Cytokine assays

Cells were seeded in 24-well-plates at 4×10^3 cells/cm^2 density and after treatments, the supernatants were retrieved and centrifuged to remove cells and debris. The samples (100 µL) were added into 96-well plates and the production of the cytokines (TNF-α, IL-6, IL-1β and IL-10) was assessed by commercial kits according to the manufacturer's instructions. The absorbance at 450 and 405 nm for TNF-α, IL-6, IL-1β and IL-10, respectively, was read by means of a microplate reader (Tecan Infinite® 200 PRO).

2.8. Immunophenotype analysis by flow cytometry

Cells were seeded in 100 × 20 mm Petri Dishes at 4×10^3 cells/cm^2 density. For surface expression of BV-2 immunophenotype, cells were incubated with Vio-bright FITC-conjugated anti-CD16/32 (1:50, Miltenyi Biotec), PE-conjugated anti-CD86 (1:50, Miltenyi Biotec), APC-

Vio770-conjugated anti-CD40 (1:50, Miltenyi Biotec), Vioblue-conjugated anti-CD68 (1:50, Miltenyi Biotec), Viogreen-conjugated anti-CD11B (1:50, Miltenyi Biotec), APC-conjugated anti-TREM2 (1:50 RnD System), PE/cyanin7 conjugated anti-CD206 (Biolegend) for 30 min at 4 °C in the dark. The samples were washed twice using PBS with 0.09 % sodium azide and assayed by means of polychromatic flow cytometry in a Cytoflex analyzer (Beckman Coulter). The samples were analyzed using Flow Logic analysis software (Inivai Technologies). For each experiment, a minimum number of 50,000 events were analyzed.

2.9. Phagocytosis assay

For the phagocytosis assay, cells were seeded (3×10^4/well) into 48-well plates in DMEM without phenol red and 24 h after plating, cells were irradiated with 153 mJ/cm^2 UVB light. After 24 h, the medium was removed and replaced with DMEM with Aβ 1–42 FITC (2.5 µg/mL). The cells were incubated at 37 °C, 5 % CO$_2$, for 30, 60, 90 and 120 min, the respective negative control for each time was incubate at +4 °C. After incubation, the samples were placed on ice to halt phagocytosis and then washed (twice in ice-cold PBS) and resuspended in ice-cold PBS. The BV-2 were then detached using Trypsin EDTA solution and assayed by means of polychromatic flow cytometry in a Cytoflex analyzer (Beckman Coulter) [38]. The samples were analyzed using Flow Logic analysis software (Inivai Technologies). For each experiment, a minimum number of 20,000 events were analyzed.

2.10. Cell migration assay

Briefly, BV-2 cells were seeded in 100 × 20 mm Petri Dishes at 4×10^3 cells/cm^2 density, and they were irradiated with 153 mJ/cm^2 UVB light. After 24 h, the cells were detached and counted. To assess UVB light effect on BV-2 chemotaxis, we used 8.0 µm pore size culture inserts in 24-well plates. A suspension containing 2.5×10^4 cells for each condition was added in 0.5 % serum medium on the upper chamber of the transwell system, whereas medium containing 10 % serum was added into the lower chamber, as FBS was used as chemoattractant [39,40]. Cells were allowed to migrate for 24 h prior to quantitation of chemotaxis. After that time, cells on the upper and lower side of the thincert were counted by Trypan Blue exclusion test. Then, the thincert membranes were washed twice with PBS and then fixed with 4 % paraformaldehyde-PBS. Cells that migrated and attached to the under-surface of the membrane were stained with crystal violet for 15 min [41]. After the staining, the transwells were washed twice with PBS and then the upper membrane was gently dried out by means of cotton swabs to remove the excess stain [42]. Subsequently, 450 µL of a 33 % acetic acid solution was added to the upper chambers of the inserts and the plate was left on slow shaking for 15 min covered in foil to avoid light. The produced eluates on the lower chambers were transferred to a 96-well plate in duplicate and the absorbance was read at 590 nm.

2.11. Gene expression: qPCR analysis

Cells were seeded in 100 × 20 mm Petri Dishes at 4×10^3 cells/cm^2 density. Total RNA was extracted with a ReliaPrep RNA Miniprep System kit. Wonder RT cDNA Synthesis kit was used for cDNA synthesis. Transcripts were quantified by real-time quantitative PCR on an 7900HT Real-Time PCR System sequence detector Applied Biosystems (Life Technologies, Carlsbad, CA, USA) with Applied Biosystems predesigned TaqMan Gene Expression Assays. The following probes were used (assay identification numbers in parentheses): Faah (Mm00515684_m1), Actin-β (Mm04394036_g1), PTGS2 (Mm00478374_m1), Aif-1 (Mm00479862_g1).

2.12. Western blotting

Cells were seeded in 100 × 20 mm Petri Dishes at 4×10^3 cells/cm^2
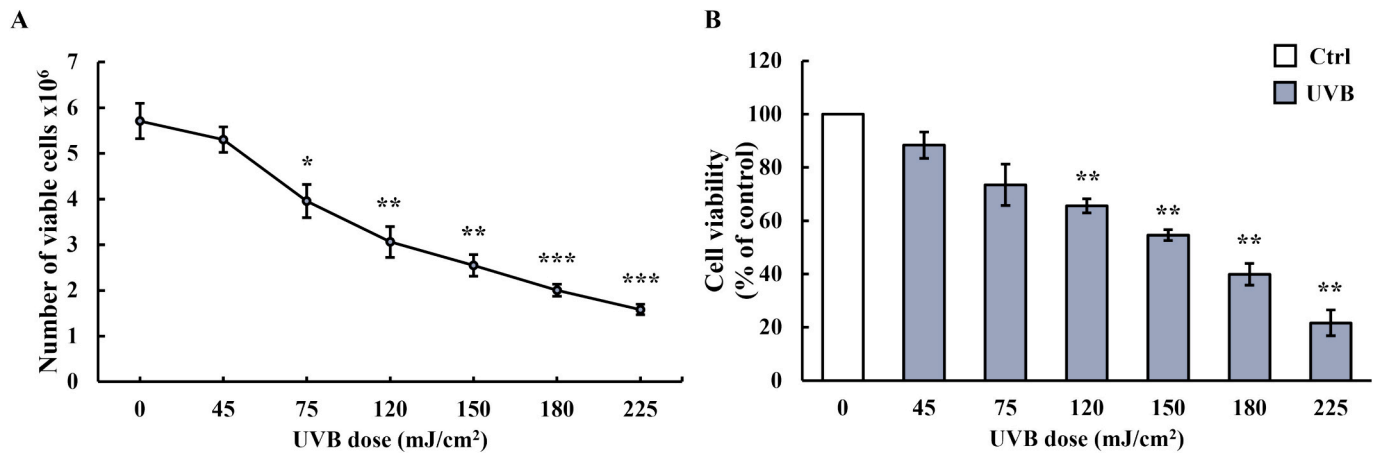
Fig. 1. Cell number and viability of BV-2 cells exposed to UVB light and tested after 24 h. (A) Cells were counted, and the number of trypan blue-negative cells was determined at the indicated UVB doses. (B) Cell viability and metabolic efficiency was tested by MTT assay. Results are expressed as mean values ± standard error of the mean (SEM) of three-five independent experiments. Significance is shown as *p* value, achieved by unpaired Student's *t*-test. $*p < 0.05$, $**p < 0.01$, $***p < 0.001$ vs. control.

density. BV-2 cells were collected after UVB treatment, washed with PBS, and lysed for 30 min at 4 °C in ice-cold RIPA buffer (50 mM Trizma base, 150 mM NaCl, 1 % Igepal, 1 mM EDTA, 1 mM EGTA, 0.1 % SDS-10 % and 0.5 % sodium deoxycholate) containing a suitable cocktail of protease and phosphatase. Equal amounts of proteins of each sample (60 μg) were separated on a 12 % SDS–polyacrylamide gel and transferred onto a polyvinylidene fluoride (PVDF) membrane. The membranes were then blocked in 5 % non-fat milk (*w/v*) and incubated with suitably diluted primary antibodies [43]. All the primary antibodies are summarized in Table S1 in the Supplementary Materials. The respective HRP-conjugated secondary antibodies were added according to the instructions. Protein bands were visualized using chemiluminescent detection system and quantified using Molecular Imager® Gel Chem-iDocTM XRS+ System (Bio-Rad Laboratories). Signal intensities were normalized to the corresponding β-actin and GAPDH levels.

2.13. FAAH activity assay

Cells were seeded in 100×20 mm Petri Dishes at 4×10^3 cells/cm^2 density. BV-2 cells were collected after UVB treatment, washed with ice-cold PBS. Enzymatic activity of FAAH, was assayed by measuring the release of arachidonic acid and of the highly fluorescent 7-amino-4-methyl coumarin (AMC) product from the non-fluorescent arachidonic 7-amino-4-methyl coumarin amide (AAMCA) [44]. All enzymatic assays were carried out at 37 °C using a pre-incubation time of 30 min. Enzyme activity was calculated as relative fluorescence units (RFU) using 15–20 μg of total protein and saturating substrate concentrations of 4 μM in a final volume of 100 μL. The cells were resuspended in Assay Buffer (50 mM Hepes pH 7.4 containing 1 mM EDTA) and subsequently sonicated for 2 s at 40 powers, this cycle was repeated 3 times. Proteins were determined according to the Bradford method. The measurements were performed with the Hitachi F-2710 Fluorescence Spectrophotometer connected to the thermostat. Adjust excitation and emission slits to 4 and 10 nm respectively, with a scanning speed of 1500 nm/min. Set the excitation wavelength at 355 nm and record fluorescence emission spectra between 350 and 600 nm (emission maximum at 460 nm) for a time interval of 60 min. A blank spectrum must be recorded and subtracted from all other spectra.

2.14. AEA, PEA, OEA 2-AG measurements

Cells were seeded in 100×20 mm Petri Dishes at 4×10^3 cells/cm^2 density. AEA, OEA, PEA and 2-AG were evaluated in BV-2 cell by ultra-high-performance liquid chromatography-tandem mass spectrometry

[45]. Briefly, the lipid fraction from BV-2 was extracted using chloroform–methanol–water (2:1:1 *v/v*) in the presence of internal standards at following concentration: AEA-d4 1 ng/mL, OEA-d4 10 ng/mL, 2-AG-d8 200 ng/mL, PEA-d4 10 ng/mL. The chloroform partition was dried under a gentle nitrogen stream and then subjected to a micro-solid phase extraction (SPE) procedure for a rapid clean-up using OMIX C18 tips from Agilent Technologies (Santa Clara, CA, USA). All analyses were performed using a Nexera XR LC 20 AD UHPLC system (Shimadzu Scientific Instruments, Columbia, MD, USA) that was equipped with Kinetex XB-C18 1.7 μm, 100 2.1 mm from Phenomenex (Torrance, CA, USA) and coupled with a 4500 Qtrap Mass spectrometry from Sciex (Toronto, ON, Canada) that was equipped with a Turbo V electrospray ionization source. The levels of the target molecules were then calculated as pmoles/10^6 cells.

2.15. Statistical analysis

Data reported in this study are the means ± standard error of the mean (SEM) of at least three independent experiments. The GraphPad Prism 8 program (GraphPad Software, La Jolla, CA, USA) was used to assess the statistical significance of differences between group means. The comparison between control and treated groups was performed by unpaired Student's *t*-test, whereas comparisons between multiple groups were performed using the one-way analysis of variance ANOVA test, followed by a Bonferroni post-hoc test. Level of $p < 0.05$ was regarded as statistically significant.

3. Results

3.1. Development and characterization of an in vitro model of sub-lethal acute UVB-induced damage in microglia

Firstly, an in vitro model of sub-lethal acute UVB injury on BV-2 cells was established. Specifically, we evaluated the effects of increasing doses of UVB exposure (i.e., 0, 45, 75, 120, 150, 180, and 225 mJ/cm^2) on cell viability and toxicity. Our findings revealed a reduction in cellular proliferation as the UVB dose increased, demonstrating a clear and direct correlation between UVB exposure and cell damage. The half-maximal inhibitory dose (ID50) for UVB irradiation was estimated at 153 mJ/cm^2, thereby serving as the benchmark dose for all successive experimental procedures (Fig. 1).

Moreover, flow cytometry analysis found that, at this dosage, UVB caused transitory alterations in BV-2 cell cycle distribution and apoptosis.
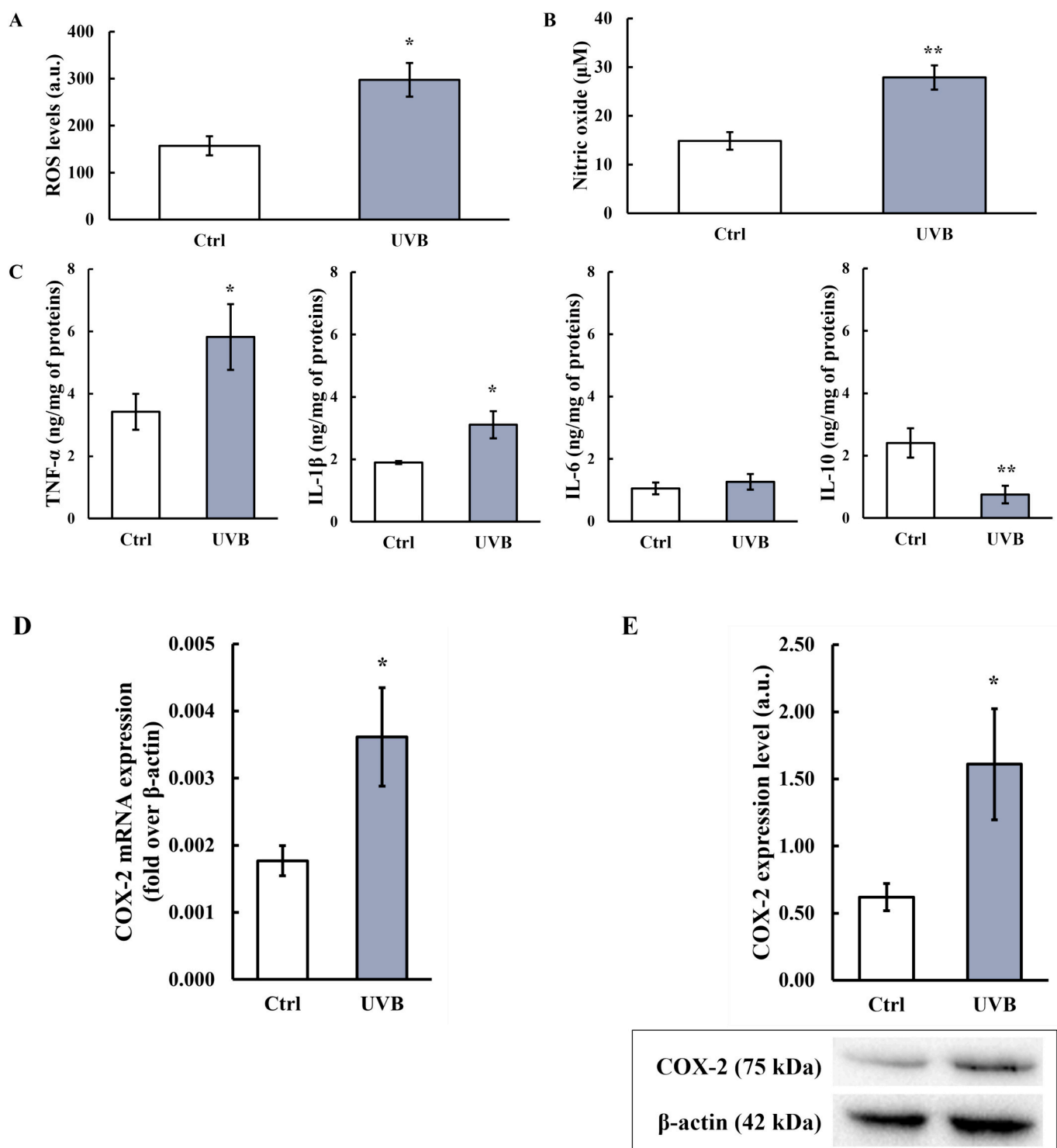
Fig. 2. ROS, nitric oxide, cytokines production and COX-2 expression in BV-2 cells. BV-2 cells were exposed to 153 mJ/cm^2 UVB dose and retrieved after 24 h. (A) Intracellular ROS were determined using 10 μM DCFH-DA at 37 °C for 30 min in darkness. Data are shown as fluorescence intensity in arbitrary units (a.u.). (B) NO content was detected using a Griess assay. (C) Released cytokines content was assessed by ELISA. (D) Expression of COX-2 was quantified for mRNA content by quantitative real-time polymerase chain reaction (qRT-PCR). (E) Expression of COX-2 was quantified for protein content by Western blotting. Equal amount of proteins (60 μg) was loaded for each sample. The blot representative image is shown below the respective graph and band density was performed by using Image-J software, normalized to β-actin. Values are expressed in arbitrary units (a.u.). Results are expressed as mean values ± standard error of the mean (SEM) of three-four independent experiments. Significance is shown as *p* value, achieved by unpaired Student's *t*-test. *$p < 0.05$, **$p < 0.01$ vs. control.

UVB irradiation induced a significant increase of the percentage of cells in G1 phase compared to control cells, indicating a cell cycle arrest. Thereby, a delay in S phase was observed in UVB-irradiated cells compared to the untreated cells(Fig. S1A). Moreover, the rate of

apoptosis was increased by 8 times because of the treatment (Fig. S1B). Notably, after 48 h of post-irradiation, cell proliferation and apoptosis levels were reported to those of control cells (Fig. S1C—D), indicating that microglial cells can heal the acute damage brought on by UVB
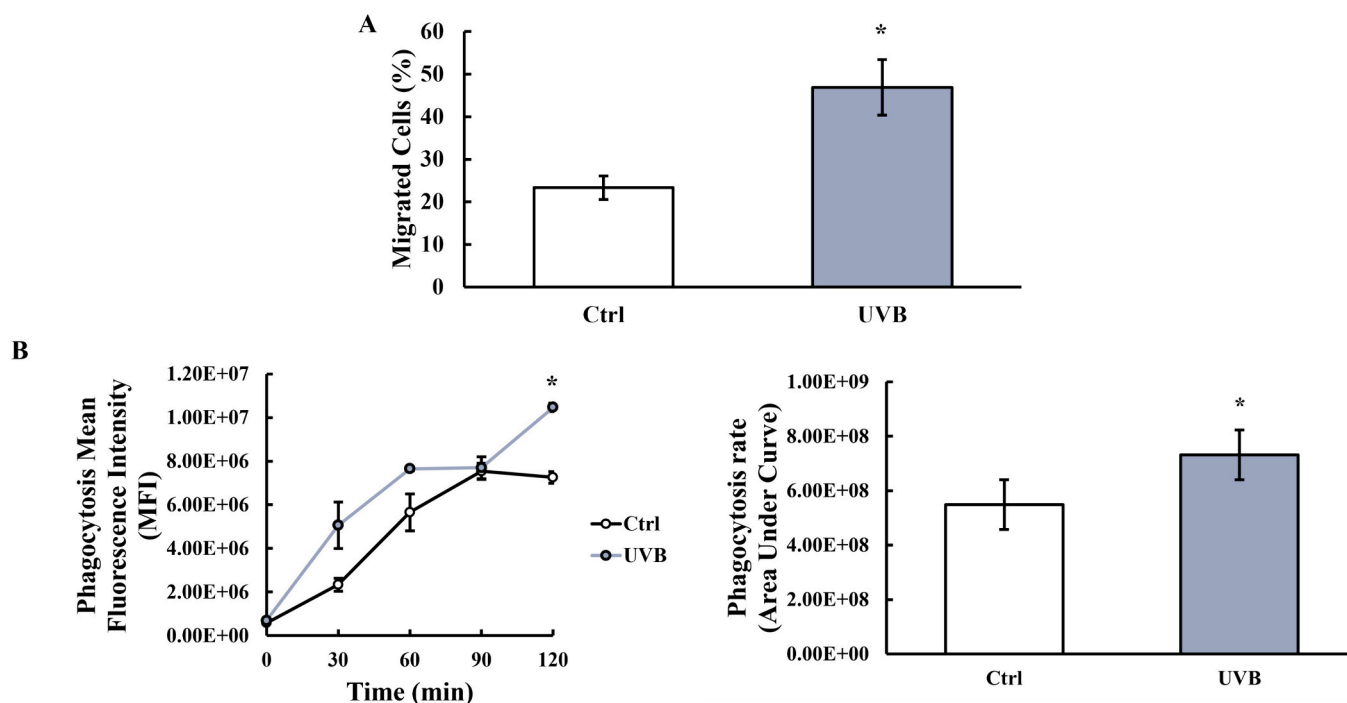
Fig. 3. UVB effect on microglia capabilities. BV-2 cells were exposed to 153 mJ/cm^2 UVB dose and retrieved after 24 h. (A) Migration was assessed by transwell migration assay and (B) Aβ 1–42 FITC phagocytosis was assessed by flow cytometry. Results are expressed as mean values ± standard error of the mean (SEM) of three independent experiments. Significance is shown as *p* value, achieved by unpaired Student's *t*-test. *$p < 0.05$ vs. control.

exposure.

To obtain more information and better characterize the role of UVB rays in modifying relevant aspects of microglial physiology, we also evaluated ROS, NO, cytokine generation along with COX-2, ionized calcium binding adapter molecule 1 (Iba-1) and immunophenotypic marker expression, as well as phagocytosis and chemotaxis.

Here, we observed that following the radiation, ROS, NO, COX −2, TNF-α and IL-1β levels all increased compared to the untreated cells. In contrast, UVB exposure markedly reduced IL-10 production, whereas no effect was obtained on IL-6 levels (Fig. 2) or Iba-1 protein expression (Fig. S2).

To ascertain whether UVB exposure also causes a change in the phenotype of cells, we evaluated by cytofluorimetry several surface markers typically associated with cells in the activated state. We observed that most of the markers tested such as CD68, CD11b, CD86, CD40, TREM2 were not affected by UVB exposure, while CD206 and CD16/32 showed a slight but significant increase in treated samples compared to unirradiated cells (Fig. S3).

Lastly, our findings indicated that irradiation increased the microglial migratory capability (Fig. 3A).

Furthermore, given the ability of microglia cells to carry out phagocytosis, we investigated whether UVB exposure would affect their ability to phagocytose FITC-conjugated Aβ1/42 peptide. Interestingly we observed an increase in phagocytosis compared to control cells (Fig. 3B) which was consistent with cell activation.

3.2. Acute UVB irradiation selectively increased the expression and activity of fatty acid amide hydrolase in microglial cells

To investigate the possible alterations in the microglial eCB signaling in UVB exposed BV-2 cells, we assessed the expression levels of the main components of the ECS by Western blotting.

No significant differences were found in the expression of the elements of the ECS (Fig. 4). On the other hand, the CB$_1$, GPR55, PPARα, PPARγ, NAPE-PLD and MAGL protein expression was not detectable.

Next, to assess the potential involvement of FAAH in the responses

observed after irradiation we measured mRNA, protein expression and enzymatic activity. As shown in Fig. 5, UVB-irradiated microglia showed a significant increase in FAAH, the primary enzyme responsible for AEA breakdown, which was ~30 % more expressed than in untreated microglia (Ctrl: 0.646 ± 0.086 a.u.; UVB: 0.842 ± 0.023 a.u.; p = 0.049).

These findings imply that acute UVB irradiation selectively elevated FAAH protein expression and activity in microglial cells, potentially lowering AEA-mediated signaling. Consistently, we found that UVB-irradiated microglia showed a significant decrease in the levels of AEA, as well as of its congeners PEA and OEA, but not of 2-AG (Table 1).

3.3. Effects of pharmacological inhibition of fatty acid amide hydrolase on the UVB-induced damage in microglial cells

To examine the possible contribution of AEA to counterbalancing UVB-induced cellular changes in BV-2 cells, we increased endogenous AEA signaling by employing URB597, a highly effective and selective FAAH inhibitor which is largely employed both in vivo and in vitro experiments [46,47]. Immediately after irradiation, the cells were treated with 5 μM URB597. This treatment fully reverted the UVB-induced reduction in the AEA levels, as well as in the levels of PEA and OEA (Table 1). With respect to UVB treated cells, the presence of URB597 significantly enhanced cell viability as showed in Fig. S4.

Moreover, URB597 significantly decreased ROS levels compared to UVB alone (Fig. 6A), reaching values comparable to the control and attenuated NO release.

FAAH inhibition also attenuated the release of TNF-α and IL-1β, with respect to the irradiated cells, while URB treatment increased the IL-10 production compared to the UVB-treated BV-2 cells (Fig. 6C). Remarkably, URB597 treatment fully reversed the effect of UVB on the changes in IL-1β and IL-10, which returned to the levels of untreated cells. URB597 addition after irradiation certainly tends to decrease COX-2 gene and protein expression, but these values did not reach statistical significance compared to irradiated cells (Fig. 6D-E). As for the Iba-1 protein expression, FAAH inhibition did not have any effect (Fig. S5).
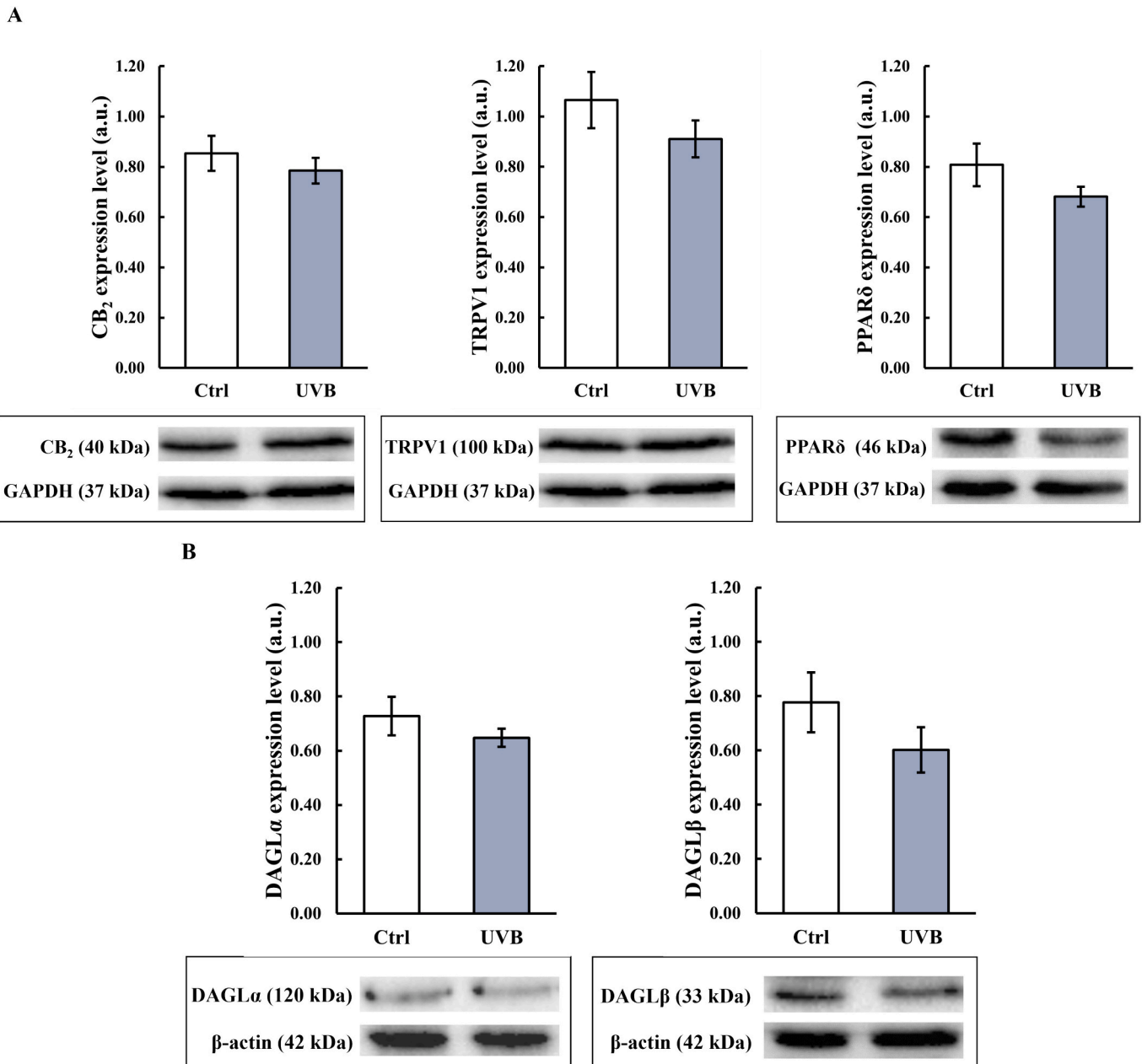
A

B

Fig. 4. Expression of eCB proteins in BV-2 cells exposed to 153 mJ/cm^2 UVB dose and retrieved after 24 h. The blot representative images of (A) receptors and (B) metabolic enzymes are shown below the respective graphs. Equal amount of proteins (60 μg) was loaded for each sample. Band density was performed by using Image-J software, normalized to GAPDH and β-actin. Values are expressed in arbitrary units (a.u.) and are the means ± standard error of the mean (SEM) of four independent experiments.

Lastly, URB597 treatment reduced the migratory rate of UVB-exposed microglia cells (Fig. 7A), but had no effect on their phagocytic activity (Fig. 7B).

4. Discussion

We established and characterized an in vitro model of sub-lethal acute UVB-induced damage in BV-2 cells, an immortalized mouse microglial cell line. Following 24 h upon UVB exposure, these cells showed: (*i*) elevated oxidative stress markers (ROS and NO), (*ii*) enhanced phagocytic and chemotactic activities, and (*iii*) altered immune profiling. Additionally, changes were observed in the expression of some components of the ECS within irradiated cells. Notably, UVB exposure led to significant upregulation of FAAH enzymatic activity, the main catabolic enzyme for fatty acid ethanolamides, along with

downregulation of AEA, PEA and OEA. Critically, FAAH inhibition via URB597 administration partially counteracted these effects, implying the potential for enhanced fatty acid amides signaling in mitigating sub-lethal UVB-induced cellular damage.

In this study, the relatively low dose of UVB induced damages that BV-2 cells successfully repaired within 48 h post-exposure. Alterations observed at 24 h post-UVB exposure, namely the elevated levels of ROS and NO, displayed an increment in COX-2, TNF-α and IL-1β expression, coupled with diminished IL-10 levels, moderately mirroring the microglial cells activation towards an M1-like or pro-inflammatory phenotype [14,48–50]. The absence of a rise in IL-6 levels in the irradiated cells and the findings on the phenotype investigation demonstrate that our cell model lacks a dominant phenotype.

Altogether, our findings reinforce the idea of a no longer quiescent microglia, but an activated one [51]. Collectively, our results imply that
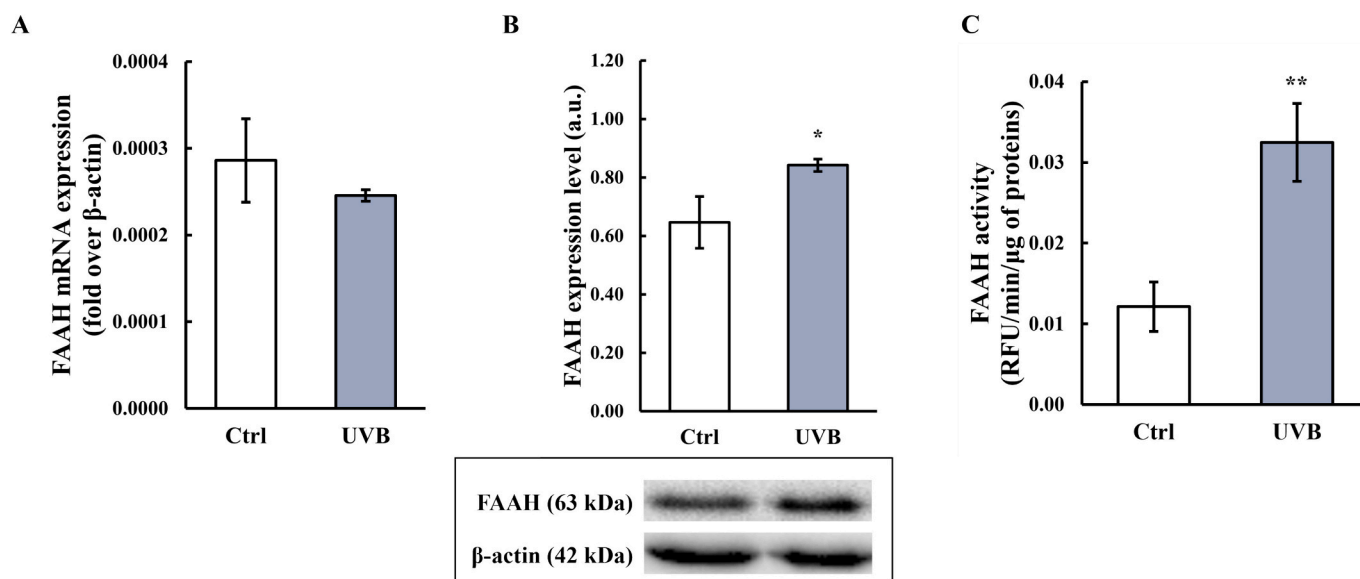
Fig. 5. UVB effect on FAAH expression and activity in BV-2 cells exposed to 153 mJ/cm^2 UVB dose and retrieved after 24 h. (A) BV-2 cells were quantified for mRNA content by quantitative real-time polymerase chain reaction (qRT-PCR). Data were shown as mean values ± standard error of the mean (SEM) of five independent experiments. (B) Expression of FAAH was quantified for protein content by Western blotting. Equal amount of proteins (60 μg) was loaded for each sample. The blot representative image is shown below the respective graph and band density was performed by using Image-J software, normalized to β-actin. Values are expressed in arbitrary units (a.u.). Data were shown as mean values ± standard error of the mean (SEM) of four independent experiments. (C) Enzyme activity was measured by fluorescence assay and data are shown as Relative Fluorescence Unit (RFU). Results are expressed as mean values ± standard error of the mean (SEM) of three independent experiments. Significance is shown as p value, achieved by unpaired Student's t-test. *p < 0.05, **p < 0.01 vs. control.

Table 1
Levels of AEA, PEA, OEA and 2-AG measured in BV-2 cells.

Lipid (pmol/ 10^6 cells)	Treatment			
	Ctrl	UVB	URB597	UVB + URB597
AEA	0.019 ± 0.004	0.005 ± 0.002*	0.037 ± 0.009**	0.032 ± 0.007####
PEA	2.3 ± 0.4	1.0 ± 0.3**	4.2 ± 0.4**	3.9 ± 1.1####
OEA	4.5 ± 1.1	1.2 ± 0.5*	8.0 ± 2.5*	7.5 ± 2.3###
2-AG	34 ± 15	35 ± 13	30 ± 17	32 ± 9

Values are expressed as mean ± standard deviation (SD) of four-five samples per group. Significance is shown as p value, calculated using One-way ANOVA followed by Bonferroni post-hoc test for multiple comparisons.

* p < 0.05
** p < 0.01 vs. control
p < 0.001
p < 0.0001 vs. UVB

a sub-lethal dose of UVB radiation represents a physical stressor that elicits a unique cellular response in microglia leading to increased levels of specific inflammatory mediators, albeit preserving the cellular functionality. We believe these characteristics warrant further and more targeted investigations in future studies.

Regarding the UV-induced changes within the microglial ECS, we found a selective increment in FAAH protein expression, and an even more substantial rise in its enzymatic activity. This was accompanied by a robust reduction in the basal levels of fatty acid N-ethanolamines, of which AEA is the prototypical member. Notably, our findings indicate that, despite a modest increase in protein expression, UVB irradiation strongly stimulates FAAH enzymatic activity, resulting in a 2.7-fold increase (Fig. 5). This variation suggests the involvement of allosteric and/or covalent mechanisms induced by UVB irradiation. In support of this possibility, FAAH has been described as a dimeric enzyme with allosteric properties [52]. Additionally, UVB irradiation significantly stimulated the expression of COX-2, increasing it by approximately 2-fold compared to untreated cells (Fig. 2). Given that COX-2 may oxidize AEA as a substrate [27,28], this upregulation could contribute to the

pronounced reduction in AEA levels that we observed in our cell model.

To assess the potential involvement of signaling mediated by these bioactive lipids in microglial response to UVB stress, we inhibited FAAH, their main degrading enzyme, by URB597. Remarkably, we observed that the rise in AEA, PEA, and OEA levels induced by URB597 was associated to counteracting the effects of UV irradiation. Our findings suggest that these lipids may contribute to mitigate several changes induced by UV irradiation, implying that enhancing of fatty acid amide-mediated signaling could improve, at least in part, the cell response to sub-lethal UVB-induced damage.

Of note, the capability of URB597 to reduce the production of ROS and NO following irradiation aligns with earlier findings on FAAH inhibition in Aβ-challenged BV-2 cells [47], primary microglia [53] and brain endothelial cells [54]. In this context, the enhancement in AEA signaling alleviated neuroinflammation through the CB$_2$-activated pathway [53], suppressed the production of TNF-α, IL-1β, and IL-6 [55,56], and increased IL-10 in activated microglia [57]. Here, we demonstrated that FAAH inhibition produced a protective effect by increasing IL-10 levels, while reducing all inflammatory mediators including COX-2, by bringing IL-1β and ROS back to the levels of unirradiated cells. These findings support those previously reported in LPS-stimulated BV-2 cells [30], positioning URB597 as a promising antioxidant and anti-inflammatory drug for protecting retinal microglia from the negative effects of UV radiation.

In conclusion, our findings indicate that the inhibition of FAAH activity via URB597 treatment could alter the cellular responses induced by UVB irradiation in microglial cells. Although additional research is needed to fully understand the molecular and cellular mechanisms at play and the potential therapeutic benefits of targeting FAAH in UVB-induced responses in microglia, our data indicate that enhancing fatty acid ethanolamides signaling through pharmacological measures might provide a protective effect, potentially assisting microglial cells in mitigating the harmful effects of sub-lethal UVB exposure. Recent studies on the skin and eyes have shifted the research focus towards examining the impact of light on brain cells [58,59], as well as its influence on microglia's role in modulating immune response [60–62]. In
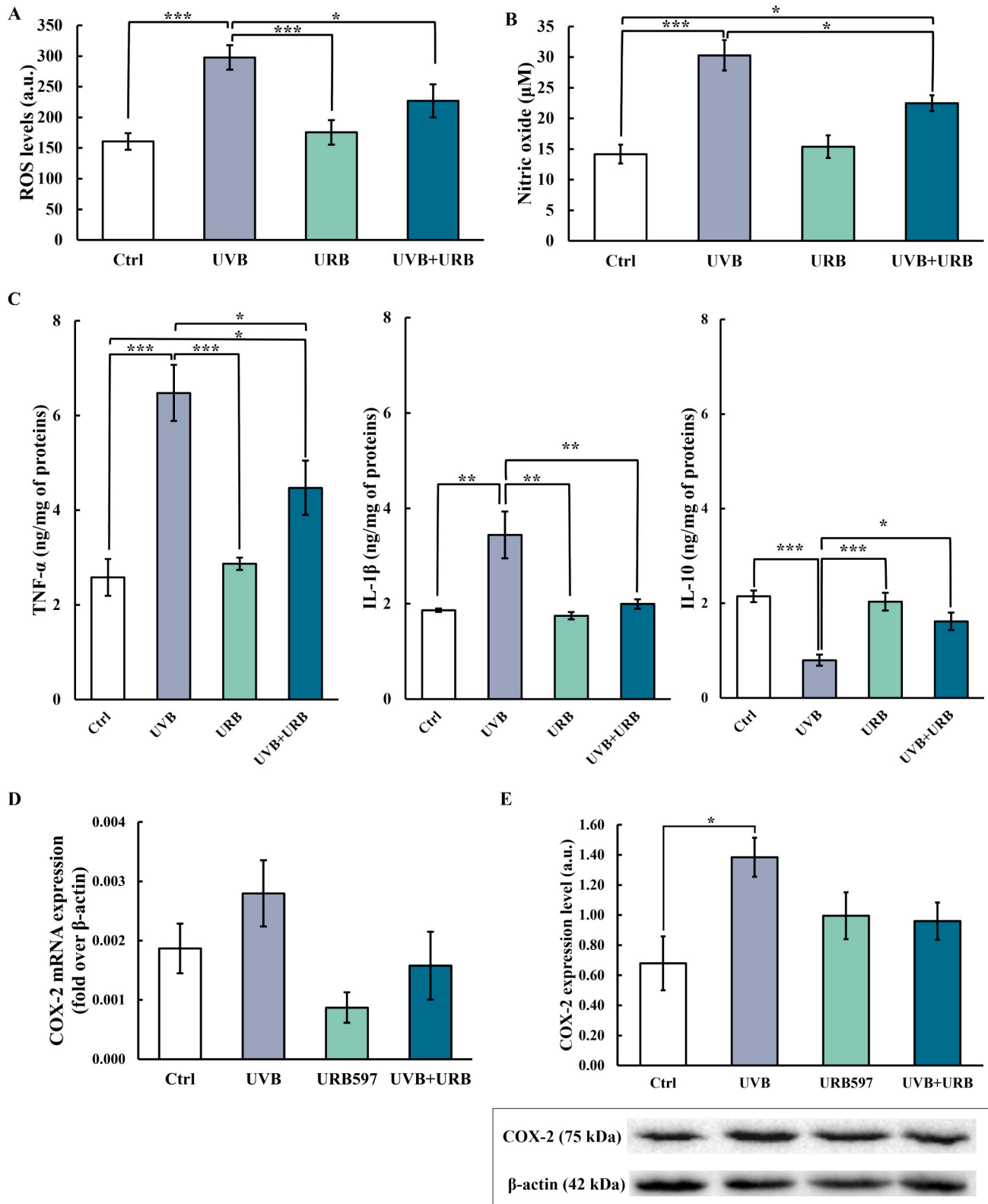
Fig. 6. Pharmacological FAAH inhibition reduces inflammatory mediators levels. BV-2 cells were irradiated with 153 mJ/cm^2 UVB dose, treated with 5 μM URB597 and retrieved after 24 h. (A) Intracellular ROS were determined using 10 μM DCFH-DA at 37 °C for 30 min in darkness. Data are shown as fluorescence intensity in arbitrary units (a.u.). (B) NO content was detected using a Griess assay. (C) Released cytokines content was assessed by ELISA. (D) Expression of COX-2 was quantified for mRNA content by quantitative real-time polymerase chain reaction (qRT-PCR). Results are expressed as mean values ± standard error of the mean (SEM) of seven independent experiments. (E) Expression of COX-2 protein was quantified by Western blotting. Equal amount of proteins (60 μg) was loaded for each sample. The blot representative image is shown below the respective graph and band density was performed by using Image-J software, normalized to β-actin. Results are expressed as mean values ± standard error of the mean (SEM) of four independent experiments and values are expressed in arbitrary units (a.u.). Significance is shown as *p* value, achieved One-way ANOVA followed by Bonferroni post-hoc test. *p < 0.05, **p < 0.01, ***p < 0.001.
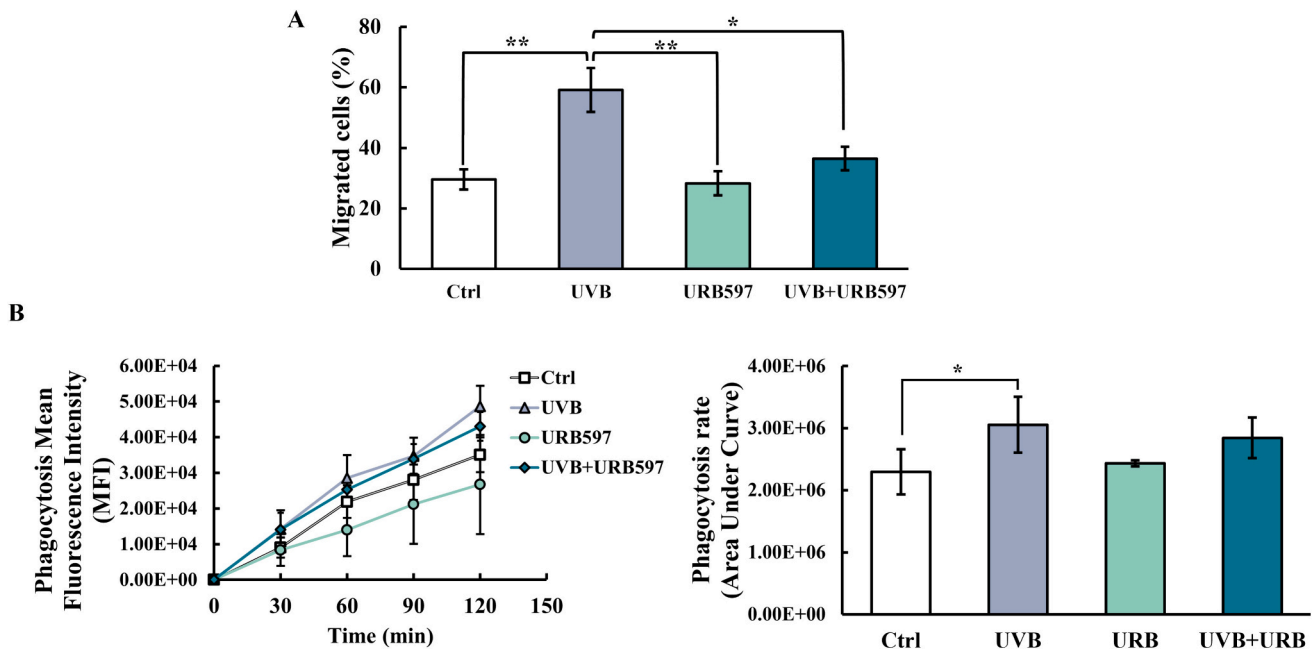
Fig. 7. Effect of URB597 on microglia capabilities. BV-2 cells were irradiated with 153 mJ/cm^2 UVB dose, treated with 5 μM URB597 and retrieved after 24 h. (A) Migration was assessed by transwell migration assay and (B) Aβ 1–42 FITC phagocytosis was assessed by flow cytometry. Values are shown as the mean values ± standard error of the mean (SEM) of three-five independent experiments. Significance is shown as *p* value, achieved One-way ANOVA followed by Bonferroni post-hoc test. *$p < 0.05$, **$p < 0.01$.

this regard, our investigation on immortalized microglia provides an initial step towards understanding the role of certain ECS components in UV light-associated neurodegenerative diseases with important implications from a translational perspective.

CRediT authorship contribution statement

Veronica Carnicelli: Writing – review & editing, Writing – original draft, Validation, Methodology, Investigation, Formal analysis, Data curation, Conceptualization. **Noemi De Dominicis:** Writing – review & editing, Software, Investigation, Data curation. **Lucia Scipioni:** Methodology, Investigation. **Marina Fava:** Methodology, Investigation. **Federico Fanti:** Methodology. **Benedetta Cinque:** Methodology, Investigation. **Alessandro Leuti:** Methodology, Investigation, Data curation. **Clotilde Beatrice Angelucci:** Methodology. **Anna Rita Lizzi:** Investigation. **Roberto Giacominelli-Stuffler:** Investigation. **Vincenzo Flati:** Investigation. **Manuel Sergi:** Methodology. **Dario Compagnone:** Validation. **Anna Maria Sardanelli:** Writing – review & editing, Methodology, Funding acquisition. **Annamaria Tisi:** Writing – review & editing. **Sergio Oddi:** Writing – review & editing, Validation, Supervision, Funding acquisition, Conceptualization. **Mauro Maccarrone:** Validation, Supervision, Funding acquisition, Conceptualization.

Declaration of competing interest

The authors declare that they have no known competing financial interests or personal relationships that could have appeared to influence the work reported in this paper.

Data availability

Data are contained within the article.

Appendix A. Supplementary data

Supplementary data to this article can be found online at https://doi.org/10.1016/j.bbalip.2024.159524.

References

[1] C.S. Subhramanyam, C. Wang, Q. Hu, S.T. Dheen, Microglia-mediated Neuroinflammation in neurodegenerative diseases, Semin. Cell Dev. Biol. 94 (2019) 112–120, https://doi.org/10.1016/j.semcdb.2019.05.004.

[2] T. Asveda, P. Talwar, P. Ravanan, Exploring microglia and their phenomenal concatenation of stress responses in neurodegenerative disorders, Life Sci. 328 (2023) 121920, https://doi.org/10.1016/j.lfs.2023.121920.

[3] S.K. Maurya, S. Gupta, R. Mishra, Transcriptional and epigenetic regulation of microglia in maintenance of brain homeostasis and neurodegeneration, Front. Mol. Neurosci. 15 (2023) 1072046, https://doi.org/10.3389/fnmol.2022.1072046.

[4] A.P. Young, E.M. Denovan-Wright, The dynamic role of microglia and the endocannabinoid system in Neuroinflammation, Front. Pharmacol. 12 (2022) 806417, https://doi.org/10.3389/fphar.2021.806417.

[5] S.J. Karlen, E.B. Miller, M.E. Burns, Microglia activation and inflammation during the death of mammalian photoreceptors, Annu Rev Vis Sci 6 (2020) 149–169, https://doi.org/10.1146/annurev-vision-121219-081730.

[6] E.B. Miller, P. Zhang, K. Ching, E.N. Pugh, M.E. Burns, In vivo imaging reveals transient microglia recruitment and functional recovery of photoreceptor signaling after injury, Proc. Natl. Acad. Sci. U. S. A. 116 (2019) 16603–16612, https://doi.org/10.1073/pnas.1903336116.

[7] E. Murenu, M.-J. Gerhardt, M. Biel, S. Michalakis, More than meets the eye: the role of microglia in healthy and diseased retina, Front. Immunol. 13 (2022) 1006897, https://doi.org/10.3389/fimmu.2022.1006897.

[8] A.T. Slominski, Ultraviolet radiation (UVR) activates central neuro-endocrine-immune system, Photodermatol. Photoimmunol. Photomed. 31 (2015) 121–123, https://doi.org/10.1111/phpp.12165.

[9] K. Rashid, I. Akhtar-Schaefer, T. Langmann, Microglia in Retinal Degeneration, Front. Immunol. 10 (2019).

[10] A. Tisi, G. Carozza, A. Leuti, R. Maccarone, M. Maccarrone, Dysregulation of Resolvin E1 metabolism and signaling in a light-damage model of age-related macular degeneration, Int. J. Mol. Sci. 24 (2023) 6749, https://doi.org/10.3390/ijms24076749.

[11] A. Tisi, M. Passacantando, M. Ciancaglini, R. Maccarone, Nanoceria neuroprotective effects in the light-damaged retina: a focus on retinal function and microglia activation, Exp. Eye Res. 188 (2019) 107797, https://doi.org/10.1016/j.exer.2019.107797.

[12] W.A. Devane, L. Hanuš, A. Breuer, R.G. Pertwee, L.A. Stevenson, G. Griffin, D. Gibson, A. Mandelbaum, A. Etinger, R. Mechoulam, Isolation and structure of a brain constituent that binds to the cannabinoid receptor, Science 258 (1992) 1946–1949, https://doi.org/10.1126/science.1470919.

[13] R. Mechoulam, S. Ben-Shabat, L. Hanus, M. Ligumsky, N.E. Kaminski, A.R. Schatz, A. Gopher, S. Almog, B.R. Martin, D.R. Compton, et al., Identification of an endogenous 2-Monoglyceride, present in canine gut, that binds to cannabinoid receptors, Biochem. Pharmacol. 50 (1995) 83–90, https://doi.org/10.1016/0006-2952(95)00109-D.

[14] L. Scipioni, F. Ciaramellano, V. Carnicelli, A. Leuti, A.R. Lizzi, N. De Dominicis, S. Oddi, M. Maccarrone, Microglial Endocannabinoid Signalling in AD. *Cells* 11 (2022) 1237, https://doi.org/10.3390/cells11071237.

[15] M. Maccarrone, V. Di Marzo, J. Gertsch, U. Grether, A.C. Howlett, T. Hua, A. Makriyannis, D. Piomelli, N. Ueda, M. Van Der Stelt, Goods and Bads of the endocannabinoid system as a therapeutic target: lessons learned after 30 years, Pharmacol. Rev. 75 (2023) 885–958, https://doi.org/10.1124/pharmrev.122.000600.

[16] A. Leuti, D. Fazio, M. Fava, A. Piccoli, S. Oddi, M. Maccarrone, Bioactive lipids, inflammation and chronic diseases, Adv. Drug Deliv. Rev. 159 (2020) 133–169, https://doi.org/10.1016/j.addr.2020.06.028.

[17] J.L. Blankman, B.F. Cravatt, Chemical probes of endocannabinoid metabolism, Pharmacol. Rev. 65 (2013) 849–871, https://doi.org/10.1124/pr.112.006387.

[18] Binte Mustafiz, S.S.; Uyama, T.; Morito, K.; Takahashi, N.; Kawai, K.; Hussain, Z.; Tsuboi, K.; Araki, N.; Yamamoto, K.; Tanaka, T.; et al. Intracellular Ca2+-dependent formation of *N*-acyl-phosphatidylethanolamines by human cytosolic phospholipase A2ε. *Biochimica et Biophysica Acta (BBA) - molecular and cell biology of* Lipids 2019, *1864*, 158515, doi:https://doi.org/10.1016/j.bbalip.2019.158515.

[19] V. Di Marzo, The endocannabinoid system: its general strategy of action, tools for its pharmacological manipulation and potential therapeutic exploitation, Pharmacol. Res. 60 (2009) 77–84, https://doi.org/10.1016/j.phrs.2009.02.010.

[20] B.Q. Wei, T.S. Mikkelsen, M.K. McKinney, E.S. Lander, B.F. Cravatt, A second fatty acid amide hydrolase with variable distribution among placental mammals*, J. Biol. Chem. 281 (2006) 36569–36578, https://doi.org/10.1074/jbc.M606646200.

[21] M. Kaczocha, S.T. Glaser, J. Chae, D.A. Brown, D.G. Deutsch, Lipid droplets are novel sites of N-Acylethanolamine inactivation by fatty acid amide Hydrolase-2, J. Biol. Chem. 285 (2010) 2796–2806, https://doi.org/10.1074/jbc.M109.058461.

[22] L. Yang, C. Ji, Y. Li, F. Hu, F. Zhang, H. Zhang, L. Li, J. Ren, Z. Wang, Y. Qiu, Natural potent NAAA inhibitor Atractylodin counteracts LPS-induced microglial activation, Front. Pharmacol. 11 (2020) 577319, https://doi.org/10.3389/fphar.2020.577319.

[23] K. Tsuboi, Y.-X. Sun, Y. Okamoto, N. Araki, T. Tonai, N. Ueda, Molecular characterization of *N*-Acylethanolamine-hydrolyzing acid amidase, a novel member of the Choloylglycine hydrolase family with structural and functional similarity to acid ceramidase*, J. Biol. Chem. 280 (2005) 11082–11092, https://doi.org/10.1074/jbc.M413473200.

[24] N. Battista, M. Di Tommaso, M. Bari, M. Maccarrone, The endocannabinoid system: An overview, Front. Behav. Neurosci. 6 (2012), https://doi.org/10.3389/fnbeh.2012.00009.

[25] T. Bisogno, F. Howell, G. Williams, A. Minassi, M.G. Cascio, A. Ligresti, I. Matias, A. Schiano-Moriello, P. Paul, E.-J. Williams, et al., Cloning of the first Sn1-DAG lipases points to the spatial and temporal regulation of endocannabinoid signaling in the brain, J. Cell Biol. 163 (2003) 463–468, https://doi.org/10.1083/jcb.200305129.

[26] T.P. Dinh, D. Carpenter, F.M. Leslie, T.F. Freund, I. Katona, S.L. Sensi, S. Kathuria, D. Piomelli, Brain Monoglyceride lipase participating in endocannabinoid inactivation, Proc. Natl. Acad. Sci. U. S. A. 99 (2002) 10819–10824, https://doi.org/10.1073/pnas.152334899.

[27] S. Valdeolivas, M.R. Pazos, T. Bisogno, F. Piscitelli, F.A. Iannotti, M. Allarà, O. Sagredo, V. Di Marzo, J. Fernández-Ruiz, The inhibition of 2-Arachidonoyl-glycerol (2-AG) biosynthesis, rather than enhancing striatal damage, protects striatal neurons from malonate-induced death: a potential role of Cyclooxygenase-2-dependent metabolism of 2-AG, Cell Death Dis. 4 (2013) e862, https://doi.org/10.1038/cddis.2013.387.

[28] K.R. Kozak, B.C. Crews, J.D. Morrow, L.-H. Wang, Y.H. Ma, R. Weinander, P.-J. Jakobsson, L.J. Marnett, Metabolism of the endocannabinoids, 2-Arachidonylglycerol and anandamide, into prostaglandin, thromboxane, and prostacyclin glycerol esters and Ethanolamides*, J. Biol. Chem. 277 (2002) 44877–44885, https://doi.org/10.1074/jbc.M206788200.

[29] S.S. Duffy, J.P. Hayes, N.T. Fiore, G. Moalem-Taylor, The cannabinoid system and microglia in health and disease, Neuropharmacol. 190 (2021) 108555, https://doi.org/10.1016/j.neuropharm.2021.108555.

[30] M. Tanaka, K. Yagyu, S. Sackett, Y. Zhang, Anti-inflammatory effects by pharmacological inhibition or knockdown of fatty acid amide hydrolase in BV2 microglial cells, Cells 8 (2019) 491, https://doi.org/10.3390/cells8050491.

[31] N. Malek, M. Kostrzewa, W. Makuch, A. Pajak, M. Kucharczyk, F. Piscitelli, B. Przewlocka, V. Di Marzo, K. Starowicz, The multiplicity of spinal AA-5-HT anti-nociceptive action in a rat model of neuropathic pain, Pharmacol. Res. 111 (2016) 251–263, https://doi.org/10.1016/j.phrs.2016.06.012.

[32] E. Rangel-López, A.L. Colín-González, A.L. Paz-Loyola, E. Pinzón, I. Torres, I. N. Serratos, P. Castellanos, M. Wajner, D.O. Souza, A. Santamaría, Cannabinoid receptor agonists reduce the short-term mitochondrial dysfunction and oxidative stress linked to excitotoxicity in the rat brain, Neuroscience 285 (2015) 97–106, https://doi.org/10.1016/j.neuroscience.2014.11.016.

[33] Á. Angyal, Z. Pénzes, S. Alimohammadi, D. Horváth, L. Takács, G. Vereb, B. Zsebik, T. Bíró, K.F. Tóth, E. Lisztes, et al., Anandamide concentration-dependently modulates toll-like receptor 3 Agonism or UVB-induced inflammatory response of human corneal epithelial cells, Int. J. Mol. Sci. 22 (2021) 7776, https://doi.org/10.3390/ijms22157776.

[34] H. Yang, Z. Wang, J.E. Capó-Aponte, F. Zhang, Z. Pan, P.S. Reinach, Epidermal growth factor receptor transactivation by the cannabinoid receptor (CB1) and transient receptor potential Vanilloid 1 (TRPV1) induces differential responses in corneal epithelial cells, Exp. Eye Res. 91 (2010) 462–471, https://doi.org/10.1016/j.exer.2010.06.022.

[35] C. Benito, E. Núñez, R.M. Tolón, E.J. Carrier, A. Rábano, C.J. Hillard, J. Romero, Cannabinoid CB2 receptors and fatty acid amide hydrolase are selectively overexpressed in Neuritic plaque-associated glia in Alzheimer's disease brains, J. Neurosci. 23 (2003) 11136–11141, https://doi.org/10.1523/JNEUROSCI.23-35-11136.2003.

[36] T. Mosmann, Rapid colorimetric assay for cellular growth and survival: application to proliferation and cytotoxicity assays, J. Immunol. Methods 65 (1983) 55–63, https://doi.org/10.1016/0022-1759(83)90303-4.

[37] C.P. LeBel, H. Ischiropoulos, S.C. Bondy, Evaluation of the probe 2′,7′-Dichlorofluorescin as an Indicator of reactive oxygen species formation and oxidative stress, Chem. Res. Toxicol. 5 (1992) 227–231, https://doi.org/10.1021/tx00026a012.

[38] S.-H. Chen, D.-Y. Tian, Y.-Y. Shen, Y. Cheng, D.-Y. Fan, H.-L. Sun, C.-Y. He, P.-Y. Sun, X.-L. Bu, F. Zeng, et al., Amyloid-Beta uptake by blood monocytes is reduced with ageing and Alzheimer's disease, Transl. Psychiatry 10 (2020) 423, https://doi.org/10.1038/s41398-020-01113-9.

[39] Y. He, X. Yao, N. Taylor, Y. Bai, T. Lovenberg, A. Bhattacharya, RNA sequencing analysis reveals quiescent microglia isolation methods from postnatal mouse brains and limitations of BV2 cells, J. Neuroinflammation 15 (2018) 153, https://doi.org/10.1186/s12974-018-1195-4.

[40] S.S. Omar Zaki, L. Kanesan, M.Y.D. Leong, S. Vidyadaran, The influence of serum-supplemented culture Media in a Transwell Migration Assay, Cell Biol. Int. 43 (2019) 1201–1204, https://doi.org/10.1002/cbin.11122.

[41] X. Zhang, P. Ye, D. Wang, Y. Liu, L. Cao, Y. Wang, Y. Xu, C. Zhu, Involvement of RhoA/ROCK signaling in Aβ-induced chemotaxis, cytotoxicity and inflammatory response of microglial BV2 cells, Cell. Mol. Neurobiol. 39 (2019) 637–650, https://doi.org/10.1007/s10571-019-00668-6.

[42] J. Pijuan, C. Barceló, D.F. Moreno, O. Maiques, P. Sisó, R.M. Marti, A. Macià, A. Panosa, In vitro cell migration, invasion, and adhesion assays: from cell imaging to data analysis, Front. Cell Dev. Biol. 7 (2019) 107, https://doi.org/10.3389/fcell.2019.00107.

[43] R. Sule, G. Rivera, A.V. Gomes, Western blotting (immunoblotting): history, theory, uses, Protocol and Problems. BioTechniques 75 (2023) 99–114, https://doi.org/10.2144/btn-2022-0034.

[44] Angelucci, C.B.; Giacominelli-Stuffler, R.; Maccarrone, M. Fluorimetric Assay of FAAH Activity. In *Endocannabinoid Signaling: Methods and Protocols*; Maccarrone, M., Ed.; Springer US: New York, NY, 2023; pp. 249–260 ISBN 978–1–07-162728-0.

[45] F. Fanti, F. Vincenti, G. Imparato, C. Montesano, L. Scipioni, F. Ciaramellano, D. Tortolani, S. Oddi, M. Maccarrone, D. Compagnone, et al., Determination of endocannabinoids and their conjugated congeners in the brain by means of μSPE combined with UHPLC-MS/MS, Talanta 257 (2023) 124392, https://doi.org/10.1016/j.talanta.2023.124392.

[46] G. Giacovazzo, T. Bisogno, F. Piscitelli, R. Verde, S. Oddi, M. Maccarrone, R. Coccurello, Different routes to inhibit fatty acid amide hydrolase: do all roads Lead to the same place? Int. J. Mol. Sci. 20 (2019) 4503, https://doi.org/10.3390/ijms20184503.

[47] M. Grieco, M.G. De Caris, E. Maggi, F. Armeli, R. Coccurello, T. Bisogno, M. D'Erme, M. Maccarrone, P. Mancini, R. Businaro, Fatty acid amide hydrolase (FAAH) inhibition modulates amyloid-Beta-induced microglia polarization, Int. J. Mol. Sci. 22 (2021) 7711, https://doi.org/10.3390/ijms22147711.

[48] S.-F. Lau, A.K.Y. Fu, N.Y. Ip, Cytokine signaling convergence regulates the microglial state transition in Alzheimer's disease, Cell. Mol. Life Sci. 78 (2021) 4703–4712, https://doi.org/10.1007/s00018-021-03810-0.

[49] V. Chhor, T. Le Charpentier, S. Lebon, M.-V. Oré, I.L. Celador, J. Josserand, V. Degos, E. Jacotot, H. Hagberg, K. Sävman, et al., Characterization of phenotype markers and Neuronotoxic potential of polarised primary microglia in vitro, Brain Behav. Immun. 32 (2013) 70–85, https://doi.org/10.1016/j.bbi.2013.02.005.

[50] J. Li, X. Shui, R. Sun, L. Wan, B. Zhang, B. Xiao, Z. Luo, Microglial phenotypic transition: signaling pathways and influencing modulators involved in regulation in central nervous system diseases, Front. Cell. Neurosci. 15 (2021) 736310, https://doi.org/10.3389/fncel.2021.736310.

[51] Y. Ji, X. Wang, C. Kalicki, B.W. Menta, M. Baumgardner, S.J. Koppel, I. W. Weidling, J. Perez-Ortiz, H.M. Wilkins, R.H. Swerdlow, Effects of microglial cytokines on Alzheimer's-related phenomena, J. Alzheimers Dis. 67 (2019) 1021–1034, https://doi.org/10.3233/JAD-180820.

[52] E. Dainese, S. Oddi, M. Simonetti, A. Sabatucci, C.B. Angelucci, A. Ballone, B. Dufrusine, F. Fezza, G. De Fabritiis, M. Maccarrone, The endocannabinoid hydrolase FAAH is an allosteric enzyme, Sci. Rep. 10 (2020) 2292, https://doi.org/10.1038/s41598-020-59120-1.

[53] N. Malek, K. Popiolek-Barczyk, J. Mika, B. Przewlocka, K. Starowicz, Anandamide, acting via CB2 receptors, alleviates LPS-induced Neuroinflammation in rat primary microglial cultures, Neural Plast. 2015 (2015) 130639, https://doi.org/10.1155/2015/130639.

[54] D.-P. Wang, K. Kang, J. Sun, Q. Lin, Q.-L. Lv, J. Hai, URB597 and Andrographolide improve brain microvascular endothelial cell permeability and apoptosis by reducing oxidative stress and inflammation associated with activation of Nrf2 signaling in oxygen-glucose deprivation, Oxid. Med. Cell. Longev. 2022 (2022) 4139330, https://doi.org/10.1155/2022/4139330.

[55] L. Ma, J. Jia, X. Liu, F. Bai, Q. Wang, L. Xiong, Activation of murine microglial N9 cells is attenuated through cannabinoid receptor CB2 signaling, Biochem. Biophys. Res. Commun. 458 (2015) 92–97, https://doi.org/10.1016/j.bbrc.2015.01.073.

[56] P. Rivera, M.D.M. Fernández-Arjona, D. Silva-Peña, E. Blanco, A. Vargas, M. D. López-Ávalos, J.M. Grondona, A. Serrano, F.J. Pavón, F. Rodríguez De Fonseca, et al., Pharmacological blockade of fatty acid amide hydrolase (FAAH) by URB597 improves memory and changes the phenotype of hippocampal microglia despite ethanol exposure, Biochem. Pharmacol. 157 (2018) 244–257, https://doi.org/10.1016/j.bcp.2018.08.005.

[57] F. Correa, M. Hernangómez, L. Mestre, F. Loría, A. Spagnolo, F. Docagne, V. Di Marzo, C. Guaza, Anandamide enhances IL-10 production in activated microglia by targeting CB2 receptors: roles of ERK1/2, JNK, and NF-κB, Glia 58 (2010) 135–147, https://doi.org/10.1002/glia.20907.

[58] K. Hiramoto, Y. Yamate, Long-term UVA exposure to the eye compromises memory and learning ability in mice via Corticotropin-releasing hormone type 2 receptor, Int. J. Biol. Sci. 16 (2020) 2170–2179, https://doi.org/10.7150/ijbs.45967.

[59] A.T. Slominski, M.A. Zmijewski, P.M. Plonka, J.P. Szaflarski, R. Paus, How UV light touches the brain and endocrine system through skin, and why, Endocrinology 159 (2018) 1992–2007, https://doi.org/10.1210/en.2017-03230.

[60] M. Han, J.-J. Ban, J.-S. Bae, C.-Y. Shin, D.H. Lee, J.H. Chung, UV irradiation to mouse skin decreases hippocampal neurogenesis and synaptic protein expression via HPA Axis activation, Sci. Rep. 7 (2017) 15574, https://doi.org/10.1038/s41598-017-15773-z.

[61] K.-N. Yoon, Y. Kim, Y. Cui, J. Ji, G. Park, J.H. Chung, Y.-S. Lee, J.-Y. An, D.H. Lee, Chronic skin ultraviolet irradiation induces transcriptomic changes associated with microglial dysfunction in the Hippocampus, Mol. Brain 15 (2022) 102, https://doi.org/10.1186/s13041-022-00989-6.

[62] C. Skobowiat, A.E. Postlethwaite, A.T. Slominski, Skin exposure to ultraviolet B rapidly activates systemic neuroendocrine and immunosuppressive responses, Photochem. Photobiol. 93 (2017) 1008–1015, https://doi.org/10.1111/php.12642.